Uniform signal enhancement in MAS NMR of half-integer quadrupolar nuclei using quadruple-frequency sweeps

Qiyan Wang, Julien Trebosc, Yixuan Li, Olivier Lafon, Shaohui Xin, Jun Xu, Bingwen Hu, Ningdong Feng, Jean-Paul Amoureux, Feng Deng

▶ **To cite this version:**

Qiyan Wang, Julien Trebosc, Yixuan Li, Olivier Lafon, Shaohui Xin, et al.. Uniform signal enhancement in MAS NMR of half-integer quadrupolar nuclei using quadruple-frequency sweeps. Journal of Magnetic Resonance, 2018, Journal of Magnetic Resonance, 293, pp.92-103. 10.1016/j.jmr.2018.06.005 . hal-04330153

HAL Id: hal-04330153
https://hal.univ-lille.fr/hal-04330153

Submitted on 7 Dec 2023

HAL is a multi-disciplinary open access archive for the deposit and dissemination of scientific research documents, whether they are published or not. The documents may come from teaching and research institutions in France or abroad, or from public or private research centers.

L'archive ouverte pluridisciplinaire **HAL**, est destinée au dépôt et à la diffusion de documents scientifiques de niveau recherche, publiés ou non, émanant des établissements d'enseignement et de recherche français ou étrangers, des laboratoires publics ou privés.

*Revised Manuscript
Click here to view linked References

Uniform signal enhancement in MAS NMR of half-integer quadrupolar nuclei using quadruple-frequency sweeps

Qiang Wang,[a,§] Julien Trébosc,[b,§] Yixuan Li,[a,b,c] Oliver Lafon,[b,e] Shaohui Xin,[a] Jun Xu,[a] Bingwen Hu,[c] Ningdong Feng,[a] Jean-Paul Amoureux,[b,c,d*] and Feng Deng[a*]

[a] *National Center for Magnetic Resonance in Wuhan, State Key Laboratory of Magnetic Resonance and Atomic and Molecular Physics, Wuhan Institute of Physics and Mathematics, Chinese Academy of Sciences, 430071 Wuhan, China.*

[b] *Univ. Lille, CNRS-8181, ENSCL, UCCS-Unit of Catalysis and Chemistry of Solids, 59000 Lille, France.*

[c] *Physics Department & Shanghai Key Laboratory of Magnetic Resonance, East China Normal University, 200062 Shanghai, China.*

[d] *Bruker Biospin, 67166 Wissembourg, France.*

[e] *Institut Universitaire de France, 75231 Paris, France.*

§ Authors with equal contributions

* Email of corresponding authors: dengf@wipm.ac.cn jean-paul.amoureux@univ-lille1.fr

Abstract

We introduce two MAS schemes that allow manipulating the satellite-transition (ST) populations of half-integer quadrupolar nuclei, and which both exhibit improved robustness to the quadruplar coupling constant (C_Q). These schemes, called quadruple frequency sweep (QFS) or quadruple WURST (QWURST) are the sums of two DFS or four WURST to efficiently invert the ST populations of nuclei subject to large or small quadrupole interactions, simultaneously. These quadruple sweeps methods only require 6% more rf-power than the double sweeps ones. We demonstrate, both numerically and experimentally, that the QFS and QWURST schemes benefit from robustness to C_Q and rf amplitude and offset and hence achieve uniform enhancement of the CT signal for ^{27}Al nuclei subject to different quadrupole interactions. Although the version of QFS with repetitive accumulation can achieve higher enhancement in the S/N of the ^{27}Al MAS spectrum, the final sensitivity gains mainly depend on the longitudinal relaxation time of different ^{27}Al sites. We also confirm that these schemes provide an improved acceleration of the ^{31}P-{^{27}Al} coherence transfer in PT-*J*-HMQC experiments.

Keywords: Half-integer quadrupolar nuclei; Quadruple-frequency sweeps; Signal enhancement; Satellite transitions; Central transition.

I. Introduction

Nuclear Magnetic Resonance (NMR) spectroscopy of half-integer spin quadrupolar nuclei, with spin number $S = n/2 \geq 3/2$, is widespread because (i) these isotopes represent about two thirds of stable NMR active nuclei and (ii) they are present in materials ranging from catalysts, glasses, ceramics and superconductors to biological systems [1-8]. In solids, the large interaction between the quadrupole moment of these isotopes and the electric field gradients splits the NMR resonance into 2*S* single-quantum transitions, which include the central transition (CT) between energy levels +1/2 and -1/2, as well as 2S - 1 satellite transitions (STs) between energy levels m and m - 1 with $m \neq 1/2$. The splitting depends on the crystallite orientation, and hence for powder samples the quadrupole interaction results in severe anisotropic broadenings, thus reducing the resolution and the sensitivity of the NMR spectra of these isotopes. The CT is not subject to the first-order quadrupole interaction, whereas STs are. Therefore, most of the time, on powder samples only the CT is observable. However, its line width can be as large as hundreds of kHz [8], and the S/N ratio hence can be very small.

Much effort has thus been devoted to the development of techniques aimed at enhancing the sensitivity of solid-state NMR experiments for half-integer quadrupolar nuclei. In particular, an ingenious and general method to increase the CT polarization, and hence the signal, consists in the manipulation of the ST populations [6b,9]. This increase can be obtained by saturating or selectively inverting the ST populations without irradiating the CT. The theoretical maximum enhancement of CT polarization is equal to S + 1/2 for the saturation and 2S for the perfect inversion of the STs converging from the external to internal transitions [10]. The maximum enhancement of 2S, corresponding to a perfect selective convergent inversion of the STs and an unaffected CT, has been achieved for spin-3/2 and -5/2 nuclei in static single crystals [11].

For static powders, the enhancements are lower because: (i) the STs cover large frequency ranges up to $3(S - 1/2)C_Q$, with $C_Q = e^2qQ$ being the quadrupolar coupling constant, and (ii) the STs always overlap with the CT and hence it is difficult to selectively excite them without perturbing the CT. Nevertheless, different schemes have been designed in order to manipulate ST populations for static powders. These schemes include the frequency-swept (SW) fast-amplitude-modulated (FAM) pulses [12], which generally lead to ST saturation, as well as the frequency swept pulses, such as the double frequency sweep (DFS) technique [13].

In the rotating frame, the DFS pulse has a constant rf-field strength ($\nu_{1\max} = \omega_{1\max}/2\pi$) and it generates two radio-frequency (rf) spikelets, which are linearly swept in a symmetric manner over a frequency interval. For static powders, DFS with a large frequency sweep range is used so that the rf-spikelets are swept from the external STs towards the CT. This convergent DFS scheme achieves an adiabatic inversion of the outer STs before the inner ones in order to reach a maximum enhancement of the CT polarization. Furthermore, for static powders the simultaneous irradiation of STs on both sides of the CT by DFS is advantageous since it inverts all STs in a twice shorter time than two sequential frequency swept irradiations on either side of the CT. Hence, DFS minimizes the losses produced by spin lattice relaxation. For static powders, DFS generally yields the best CT signal enhancement [6b]. This enhancement is below the theoretical one of 2S because: (i) the quadrupolar splitting depends on the crystallite orientation, and (ii) the frequency sweep can achieve adiabatic inversion only for crystallites exhibiting quadrupolar splittings much larger than $\nu_{1\max}$ [14]. Otherwise, i.e. for crystallites exhibiting small quadrupolar splitting, the frequency sweep does not produce the anticipated effects and the gain of CT polarization of those crystallites is lower than the theoretical one.

To enhance the resolution, Magic-Angle Spinning (MAS) of the sample is often used. For each crystallite, the frequencies of STs are modulated by the MAS frequency, ν_R, and their resonances break up into several spinning side-bands (ssbs). For frequency swept pulses, such as DFS, the effective frequency sweep is the sum of the carrier frequency sweep and the modulation of the quadrupole interaction by the

rotation. Therefore, the effective sweep frequency, and hence the enhancement of CT polarization by broadband DFS, depend on the crystallite orientation [15]. As a result, broadband DFS produces lower enhancements under MAS than under static conditions. SW (τ and $1/\tau$)-FAM [12] was also proved to generate frequencies spreading over the range of their sweep width, which could lead under MAS to a better signal enhancement than the original FAM [10]. In fact, there is no essential difference between SW-FAM and DFS from a physical point of view, since they can provide very similar results for the frequency sweep. However, due to their simple amplitude modulation, FAM and it variants can be employed on spectrometers for which frequency modulation of the very short RF pulse is not feasible.

Under MAS, an alternative to the broadband excitation is the selective irradiation of one or a few ssbs [16]. This selective irradiation can be achieved by FAM pulses, which saturate the STs. This method was also named Rotor-Assisted Population Transfer (RAPT) [17]. More conventional shaped inversion pulses, such as hyperbolic secant (HS) pulse [18] and wideband uniform-rate and smooth-truncation (WURST) [19], have been employed to irradiate ssbs of STs. In principle, the use of an adiabatic inversion pulse ensures a perfect inversion of the STs magnetization, provided the adiabaticity condition is satisfied. The largest enhancements for these frequency-swept adiabatic pulses are obtained when the width of their frequency sweep is equal to ν_R. Under such condition, enhancements in between S + ½ and 2S can been achieved, indicating that these pulses produce a partial inversion of STs under MAS. For a crystallite, the selective excitation of a single MAS ssb can theoretically produce a perfect inversion of the ssb manifold [16]. However, for some crystallites, the irradiated ssb has a very small intensity and the STs of those crystallites are not inverted. Furthermore, for nuclei with $S \geq 5/2$, the ssbs of two consecutive STs partially overlap and it is impossible to completely excite them sequentially, i.e. to invert the outer STs prior to the inner ones. Therefore, in practice, the enhancements obtained by exciting a single ssb with adiabatic inversion pulses are lower than 2S in MAS.

In addition to pulses selectively irradiating a single ssb, narrow-band DFS

selectively irradiating two ssbs symmetric about the CT has been tested [20]. Contrary to single ssb excitation, the narrow-band DFS equally affects the two symmetric STs, $m \leftrightarrow m+1$ and $-m-1 \leftrightarrow -m$. A variant of the narrow-band DFS is the sideband-selective DFS, which is obtained by modulating the amplitude of a narrow-band DFS by a sine-squared profile in order to improve the adiabaticity [21c].

In addition to the enhancement of the CT polarization, the manipulation of the STs one has been shown to accelerate coherence transfers in Heteronuclear Multiple-Quantum Correlation (HMQC) experiments with indirect detection of half-integer quadrupolar nuclei [22]. These experiments, called Population-Transfer HMQC (PT-HMQC), improve the sensitivity in cases where the hetero-nuclear J or dipolar couplings mediating the coherence transfer are smaller than the rate of transverse losses.

Nevertheless, all techniques that manipulate the populations of STs by irradiating a single or two symmetric ssbs, have a common limitation: they are sensitive to the quadrupole interaction. Indeed, the sites with large C_Q values require using ssb selective pulses with (i) large rf-field to achieve an efficient inversion and (ii) large frequency offset with respect to the CT so that the latter is not perturbed by rf irradiation. This is the contrary for sites with small C_Q values. Hence, sites with different quadrupole interactions often exhibit distinct enhancements of the CT polarization. This non-uniform gain has been used for spectral editing [21, 23].

Herein, we introduce two improved MAS schemes that allow manipulating the ST populations of half-integer quadrupolar nuclei, and which both exhibit improved robustness to the C_Q value. These schemes, called quadruple frequency sweep (QFS) or quadruple WURST (QWURST) are the sums of two sideband-selective DFS or four sideband-selective WURST with offsets and rf-fields that are both either large or small to efficiently invert the ST populations of nuclei subject to large or small quadrupole interactions, respectively. We demonstrate on crystalline aluminophosphate materials, through numerical simulations and experiments, that the QFS and QWURST schemes benefit from high robustness to C_Q and rf amplitude and offset and hence achieve uniform enhancement of the CT signal for ^{27}Al nuclei

subject to different quadrupole interactions. Similar to multiple RAPT/FAM [21a,b] and repetitive DFS [21c] strategies, repeating the QFS scheme and signal readout without allowing for longitudinal relaxation can lead to further sensitivity enhancement. However, the uniform enhancement of the CT of different ^{27}Al sites cannot be maintained due to their different T_1 relaxation times. We also show that these schemes provide an improved acceleration of the ^{31}P-^{27}Al coherence transfer in PT-*J*-HMQC experiments with the indirect detection of ^{27}Al isotopes via ^{31}P spy nuclei (^{31}P-{^{27}Al}).

II. Method

II.1 Frequency-swept pulses

During a pulse, in the rotating frame the rf-Hamiltonian is given by

$$H_{rf} = \omega_1(t)\{\cos[\phi(t)]I_x + \sin[\phi(t)]\, I_y\} \quad (1)$$

where $\omega_1(t)$ and $\phi(t)$ are the instantaneous rf amplitude and phase.

During a WURST pulse, the rf-amplitude is given by [24]:

$$\omega_1(t) = \omega_{1\max}\left[1 - \left|\cos\left(\pi\frac{t}{T_p}\right)\right|^N\right] \quad (2)$$

with $\omega_{1\max}$ the peak amplitude of the rf-field. T_p is the WURST pulse duration and the index *N* determines the extent to which the edges of the pulse are rounded off. The phase is modulated as a quadratic function of time and for a decreasing frequency sweep equal to $\nu_R = \omega_R/2\pi$, it is equal to:

$$\phi(t) = \left(\omega_{\text{off}} + \frac{\omega_R}{2}\right)t - \frac{\omega_R}{2T_p}t^2 \quad (3)$$

where $\omega_{\text{off}} = 2\pi\nu_{\text{off}}$ is the average offset angular frequency at the center of the pulse (t = T_p/2). This phase modulation can be described in a frame, known as the frequency-modulated frame [25], rotating in concert with the rf-field as a linear sweep of the carrier frequency:

$$\omega_{\text{off}}(t) = \frac{\mathrm{d}\phi}{\mathrm{d}t} = \omega_{\text{off}} + \frac{\omega_R}{2} - \frac{\omega_R}{T_p}t \quad (4)$$

In this article, we introduce double WURST (DWURST) pulses, which irradiate two symmetric sets of ST ssbs (Fig.**1b**). These pulses consist of the sum of two identical WURST pulses with peak amplitudes, $\nu_{1\max}$, and opposite offsets, $\pm\nu_{\text{off}}$. For each

species, the ssbs are situated at the sum of the isotropic chemical shift and the quadrupolar induced shift (QIS) associated to each transition, plus a multiple of ν_R. It has been shown that for the m $\leftrightarrow$ m - 1 transition, in units of $(1 + \eta_Q^2/3)\nu_Q^2/(10\nu_0)$ the QIS can be written as [2,26]:

$$QIS = 1 - I(I + 1) + 36m(m - 1)/4 \quad (5)$$

where $\nu_Q = 3C_Q/[2S(2S-1)]$ is the quadrupole frequency and 36m(m – 1) = -9, 27, 135, 315, 567 for the CT, ST_1 (inner), ST_2 (2^{nd}), ST_3 (3^{rd}) and ST_4 (4^{th}) transitions, respectively. The ssbs of the CT are often very limited in number and amplitude, and they are not relevant for the CT signal enhancement. For a given species and sideband order, the ssbs of the STs (i) are always in the same frequency order: $ST_1 < ST_2 < ST_3 < ST_4$ (Eq.5), and (ii) they cover a frequency range which is often much smaller than ν_R because the frequency difference in between ssbs of the external and internal STs is small:

$$QIS_{ext} - QIS_{ST1} = 3/128,\ 9/245 \text{ and } 243/4000 \quad (6)$$

in units of $(1 + \eta_Q^2/3)C_Q^2/\nu_0$, for S = 9/2, 7/2 and 5/2, respectively. For each species, the most efficient way to increase its CT magnetization is to irradiate one of its sets of close ssbs, and sweep it with decreasing order, i.e. from the outer ST to the inner one. Therefore, we have always swept down the frequency in the WURST, DWURST or QWURST pulses (Fig.**1b**, **d**).

The DFS pulse produces a linearly oscillating rf-field, which can be decomposed into the sum of two counter-rotating rf-fields. In the rotating frame this creates two rf-spikelets with constant amplitude, ν_{1max}, irradiating in opposite directions at $\pm\nu_{off}(t)$ with respect to the carrier frequency (Fig.**1a**). With a frequency sweep equal to ν_R, $\nu_{off}(t) = \omega_{off}(t)/2\pi$ is given by Eq.4.

In this article, we also introduce the quadruple WURST (QWURST) pulse, which consists of four WURST pulses with the same decreasing sweep to irradiate the STs by decreasing order, and with rf angular offsets and peak amplitudes of $(\pm\nu_{off},\ \nu_{1max})$ and $(\pm\nu_{off}/2,\ \nu_{1max}/4)$ (Fig.**1d**). We have chosen these two sets of rf offsets and amplitudes because they allow similar efficiencies for the ST $\rightarrow$ CT transfers of nuclei with C_{Qs} in the ratio of ca. 2, as shown by comparing Figs.**8a** and **9a** simulated

for DWURST with C_Q = 3 and 1.5 MHz, respectively. This quadruple simultaneous excitation makes the QWURST pulse robust with respect to the quadrupole interaction.

In a similar way, we also introduce the QFS pulse (Fig.**1c**), which consists of the sum of two DFS pulses with rf offsets and fields of ($\pm\nu_{\mathrm{off}}$, $\nu_{1\mathrm{max}}$) and ($\pm\nu_{\mathrm{off}}/2$, $\nu_{1\mathrm{max}}/4$), and the four rf-spikelets converging towards the CT. With DFS and QFS, only half of the STs are irradiated by decreasing order.

Note that the rf-power, which is proportional to the square of the rf-amplitude, is hence only 6% higher for the QFS and QWURST pulses than for the DFS and DWURST ones.

II.2 The employed NMR sequences

In Fig.**2a**, the previous frequency-swept pulses are used to manipulate the ST populations during T_p to enhance the CT one. Then a CT-selective pulse converts the enhanced CT polarization into a CT single-quantum coherence, which is detected during the acquisition period. Fig.**2b** represents the repetitive applications of sideband-selective QFS and acquisitions without allowing the system to relax.

These swept pulses can also be incorporated into the ^{31}P-{^{27}Al} PT-*J*-HMQC sequence in order to accelerate the ^{31}P-^{27}Al coherence transfer through the *J*-coupling. This sequence, displayed in Fig.**2c**, derives from the conventional ^{31}P-{^{27}Al} *J*-HMQC sequence, but the coherence transfer related to $J_{31\mathrm{P}\text{-}27\mathrm{Al}}$ during the defocusing and refocusing delays, τ_{mix}, is accelerated by applying M frequency-swept pulses, which manipulate the ^{27}Al ST populations [22]. Furthermore, the initial transverse ^{31}P magnetization is created herein by a ^{1}H$\rightarrow$^{31}P CPMAS scheme.

III. Details of simulations and experiments

In Fig.**4**, **5**, **9** and **10** the experimental or simulated signal has been normalized to its maximum value. All experiments and simulations were performed with a static magnetic field of B_0 = 9.4 T.

III.1. Numerical simulations

To rationalize the ST $\rightarrow$ CT transfers, numerical simulations were carried out using SIMPSON software [27]. The powder averaging was accomplished using 2460

$\{\alpha_{MR}, \beta_{MR}, \gamma_{MR}\}$ Euler angles that describe the orientation of the Molecule in the Rotor frame. The 615 $\{\alpha_{MR}, \beta_{MR}\}$ pairs were selected according to the REPULSION algorithm [28], whereas the four γ_{MR} angles were regularly stepped from 0 to 360°. The spin system was an isolated ^{31}P-^{27}Al spin pair with J = 100 Hz. The ^{27}Al quadrupole interaction was considered up to the second order with $\eta_Q = 0$ and C_Q = 3.0 (Fig.**9**) or 1.5 MHz (Fig.**10**). The other spin interactions were discarded. For all simulations, the MAS frequency was ν_R = 25 kHz. We simulated in a 1D way ($t_1 = 0$) the signal of the ^{31}P-{^{27}Al} PT-*J*-HMQC sequence (Fig.**9**,**10**), starting from the ^{31}P transverse magnetization and selecting the +1Q ^{27}Al coherence. An ideal π-pulse was employed on ^{31}P channel and the nutation frequency was 8 kHz for the two ^{27}Al CT selective π/2-pulses. The recoupling delay was fixed to τ_{mix} = 1.68 ms ≈ 1/6*J*.

III.2. Experiments

All experiments were carried out at ν_R = 15 kHz on a Bruker Avance-400 spectrometer operating with a Bruker 3.2 mm HXY probe. Acquisitions were performed by observing ^{27}Al and ^{31}P of $AlPO_4$-14 at the Larmor frequencies of 104.3 and 162.0 MHz, respectively. This sample contains three P and four Al sites exhibiting very different quadrupole coupling constants with C_Q = 1.7, 4.2, 5.6 and 2.6 MHz for Al_1, Al_2, Al_3 and Al_4, respectively [29]. This compound is thus adequate to demonstrate the advantages of quadruple frequency sweep schemes. We have also used $AlPO_4$ berlinite with a single Al site (C_Q = 4.7 MHz) as a model sample to analyze the robustness of these schemes to the average offset frequency, ν_{off} (Fig.**7**) [30].

Fig.**2a** shows the 1D pulse sequence, with a frequency sweep before the CT-selective π/2-pulse, used to measure the ^{27}Al CT signal enhancement. Fig.**2b** represents the repetitive version of QFS. Inversion recovery method was used to measure the T_1 of the different ^{27}Al sites on $AlPO_4$-14. In the case of ^{31}P-{^{27}Al} 2D experiments (Fig.**2c**), an initial $^1H \rightarrow {}^{31}P$ CPMAS transfer was used with a contact time of 3 ms and rf-fields of $\nu_{31P,CP} \approx 40$ kHz and $\nu_{1H,CP} \approx 55$ kHz (ramped). The central ^{31}P π-pulse used an rf-field of $\nu_{31P,\pi} \approx 52$ kHz, and the two ^{27}Al CT-selective

π/2-pulse-lengths were of 7.5 μs ($\nu_{27Al,\pi/2} \approx 11$ kHz). The ^{31}P resolution was enhanced with two simultaneous ^{1}H and ^{27}Al decoupling sequences. A SPINAL-64 ^{1}H decoupling, with an rf-field of 75 kHz was applied after the CP transfer, whereas during t_2 acquisition a ^{27}Al rotor-asynchronized multiple-pulse (RA-MP) decoupling [31], was also applied. This decoupling consisted of ^{27}Al pulses with rf-field strength of 40 kHz, lasting 5 μs each, and separated by windows of 83 μs. In PT-*J*-HMQC experiments, the ST → CT transfers were performed with the four different schemes depicted in Fig.**1** whose parameters (Table 1) were optimized by using the pulse sequence in Fig.**2a**. A fixed frequency sweep pulse length of T_p = 500 μs was employed and repeated M times during τ_{mix} for each experiment. The conventional *J*-HMQC experiment was obtained by removing during τ_{mix} the adiabatic frequency sweep pulses.

IV. Results and discussion

IV.1. Single pulse excitation

Actually, the application of multiple frequency sweeps has already been explored in previous studies. For example, (i) Iuga used two simultaneous broadband DFS to optimize the performance of the DFS theoretically and experimentally [15]; (ii) Siegel performed HS frequency sweeps at two different frequencies (ν_{off} and -ν_{off}/2) [18]; and (iii) the four-point FAM [10] or two subsequent FAM with different timings [12] presented by Brauniger also generated irradiations at two positive and two negative frequencies. Here, we aim to illustrate the feasibility of the combination of sideband-selective adiabatic inversion pulses and weighted rf-fields applied on different offsets in quadruple frequency sweep scheme, which should alleviate the saturation effect on the central transition of half-integer quadrupolar nuclei.

The ^{27}Al MAS spectra of $AlPO_4$-14 using the four frequency sweep schemes of Fig.**1** are shown with ν_{1max} = 26.4 kHz in Fig.**3b**-**g**. For DFS and DWURST experiments, the spectra were recorded with ν_{off} = 150 (Fig.**3d**,**f**) or 300 kHz (Fig.**3e**,**g**). In case of QFS and QWURST, we employed frequency sweeps with simultaneous offsets of ±150 and ±300 kHz (Fig.**3b**,**c**). Compared to the normal

CT-selective π/2-pulse-acquire spectrum (Fig.**3a**), the enhancement factors of the four different ^{27}Al sites with the above sweep schemes are summarized in Table 1. As discussed previously, $AlPO_4$-14 consists of four crystallographically distinct Al sites with different C_Qs which exhibit quite distinct ST ssb patterns. It is hence difficult to obtain optimal ST → CT transfers for all ^{27}Al species by just sweeping at two symmetric offsets. Indeed, using DFS and DWURST with ν_{off} = 150 kHz yields CT enhancements of ca. 2.4 for Al_1 sites, while smaller enhancements of 1.3 - 1.6 are observed for the other three sites with larger C_Q values (Table 1). Oppositely, with ν_{off} = 300 kHz one obtains gains of ca. 2.5-2.6 for the later three Al sites, but of 1.84 for Al_1 site with the smallest C_Q. On the contrary, using the QFS and QWURST quadruple sweep schemes with simultaneous offsets of ±150 and ±300 kHz, results in enhancements of ca. 2.5 ± 0.1 for all four Al sites of $AlPO_4$-14 (Table.1). It is clear that the quadruple frequency sweep schemes have improved the robustness of frequency sweep to the quadrupole interactions. Actually, the QFS and QWURST sequences can be considered as the independent combinations of two DFS and DWURST pulses, simultaneously irradiating at two sets of ST ssbs. The much lower peak rf-field amplitude of 6.6 kHz of the inner adiabatic pulses at ±150 kHz is required to avoid the interference of these two frequency sweep irradiations with the CT. It must be emphasized that the WURST shape pulse can be replaced by other adiabatic pulses, such as HS, in our quadruple frequency sweep strategy, which yield uniform sensitivity gains for the four Al sites of $AlPO_4$-14, similar to those of QWURST (results not shown).

Further experimental investigations have been done to optimize ν_{off} and $\nu_{1\text{max}}$ of the different schemes by using the pulse sequence in Fig.**2a**. The signal intensities of Al_1 and Al_3 sites as a function of ν_{off} and $\nu_{1\text{max}}$ are plotted in Fig.**4** and **5**, respectively. One observes that the optimal peak rf-field is always in the range of $\nu_{1\text{max}}$ ≈ 15-30 kHz. With DFS and DWURST, the best enhancement of Al_1 site is achieved with ν_{off} ≈ 160-200 kHz, while it decreases above this range. Due to the simultaneous irradiations at $\pm\nu_{\text{off}}$ and $\pm\nu_{\text{off}}/2$, this decrease for Al_1 is negligible with QFS and QWURST, which also allows a very good transfer for all other Al species,

even Al_3 with ν_{off} > 200 kHz. DFS and DWURST may be very slightly more efficient than QFS and QWURST for one particular species, but then this is the opposite for the other Al resonances. On the contrary, QFS and QWURST are very efficient for all Al species simultaneously. Since the purpose of this manuscript is not to obtain the most efficient method for one particular species, but for all, we will focus now our discussion on the way to make the population transfers the most robust possible versus C_Q values.

Fig.**6** displays the experimental CT enhancement factor versus ν_{off} of the four Al sites of $AlPO_4$-14 with ν_{1max} = 26.4 kHz and the four sweep schemes shown in Fig.**1**. Compared to the other three Al sites, Al_1 reveals a rather different enhancement evolution with DWURST and DFS (Fig.**6a** and **c**). It increases very fast and is maximum (ca. 2.5) with $\nu_{off} \approx$ 170 kHz, when simultaneously the gain is of only ca. 2.0 for Al_3. However, when the gain is maximum with $\nu_{off} \approx$ 300 kHz for Al_2, Al_3 and Al_4, that for Al_1 has decreased rapidly to ca. 1.8-1.9. On the contrary, QWURST and QFS make the enhancement factor build-up curves to be little C_Q dependent (Fig.**6b** and **d**). This improvement may thus offer an acceptable route to employ this ST $\rightarrow$ CT transfer strategy in some hetero-/homo- correlation MAS experiments involving half-integer quadrupolar nuclei, without significant influence of the local electric field gradients in different chemical environments.

Here, we would like to explore in more detail the robustness of these sweeping methods with respect to ν_{off} versus the total shift (isotropic chemical plus quadrupolar-induced). This analysis is difficult to perform with $AlPO_4$-14 which contains four Al species and thus four different shifts, and this sample should hence only lead to an averaged evaluation. For such an analysis, we have thus used a berlinite sample, since it only has a single aluminum site with a moderate quadrupole interaction (C_Q = 4.7 MHz). In Fig.**7** we show the signal that is observed with the frequency sweep bandwidth of ν_R = 15 kHz, and ν_{off} varied from 170 to 200 kHz with a step of $\Delta\nu_{off}$ = 1 kHz for DFS/DWURST and from 340 to 400 kHz with $\Delta\nu_{off}$ = 2 kHz for QFS/QWURST. One observes that D/Q-WURST signal is subject to a non-negligible modulation with ν_R frequency. This means that the signal depends

largely on the ν_{off} value, and hence on the experimental optimization. This is much less the case with DFS and particularly with QFS, which is very robust with respect to the particular value of ν_{off}.

IV.2. Repetitive quadruple frequency sweep

It has been demonstrated that the remaining polarization of the satellites after a single RAPT/FAM/DFS manipulation can be used to achieve a further enhancement of the CT by employing these schemes several times before waiting for the re-equilibration of the spin system.[21] Here, we have also explored the interest of repetitive manipulation for QFS. Fig.**8a** and **8b** show the experimental results obtained for $AlPO_4$-14 using a single pulse and the repetitive QFS sequence of Fig.**2b** with N = 16, respectively. Although much higher S/N gains, larger than 3.7, can be obtained with the weighted addition of the individual FIDs recorded with the repetitive QFS, a uniform enhancement cannot be maintained for the four Al sites (Fig. **8c-f**), as compared with the regular QFS scheme. Especially, after N = 16 accumulations, the Al_3 site exhibits an enhancement of ca. 4.5 (Fig.**8e**), which is 20 % higher than for the other three sites. This difference can be attributed to its much shorter relaxation time ($T_{1,Al3} \approx 6.9$ ms) compared to the others sites: $T_{1,Al1} \approx 25.9$, $T_{1,Al2} \approx 25.8$ and $T_{1,Al4} \approx 45.7$ ms. This result demonstrates that the enhancement factor is affected by the longitudinal relaxation time in the repetitive strategy.

IV.3. ^{31}P-{^{27}Al} PT-*J*-HMQC experiments

One of the main applications of the ST → CT transfer of populations is to speed up the *J*-recoupling, which is required to acquire *J*-HMQC 2D spectra, between spin-1/2 and half-integer quadrupolar nuclei. Indeed, these small *J* couplings require long mixing times, during which the signal is largely attenuated due to losses which are often important when dealing with quadrupolar nuclei. To demonstrate the feasibility of such strategy, we have first simulated the PT-*J*-HMQC ^{31}P-{^{27}Al} signal for one isolated ^{27}Al-^{31}P spin-pair with J = 100 Hz and the 4 different ST → CT transfer schemes in Fig.**1**. Two quadrupolar constants were selected for ^{27}Al, C_Q = 1.5 and 3 MHz, and this interaction was considered with η_Q = 0 to the second order. The

signal intensities of the $^{31}P \rightarrow {}^{27}Al \rightarrow {}^{31}P$ transfers are plotted in Fig.**9** and **10** for C_Q = 3 and 1.5 MHz, respectively, versus peak rf-field (ν_{1max}) and offset (ν_{off}), for the four sweep schemes. These two figures demonstrate that the QFS/QWURST schemes can cover a much broader range of ν_{off} parameter compared to conventional DFS/DWURST schemes, especially with small C_Q values (Fig.**10b**,**d**). This shows that the quadruple frequency sweep strategy is also available for our very recently developed PT-*J*-HMQC experiment.

Fig.**11** displays the ^{31}P signal observed on $AlPO_4$-14 after a $^{31}P \rightarrow {}^{27}Al \rightarrow {}^{31}P$ transfer, versus τ_{mix}, either with *J*-HMQC (Fig.**11b**) or PT-*J*-HMQC (Fig.**11a**) with the QFS sequence, as shown in Fig.**2c**. In order to show the robustness of the QFS population transfer with respect to rf-field and also to alleviate its interference with proton decoupling, we have used a peak value of only $\nu_{1max} \approx 14$ kHz. The offset was pre-optimized with the pulse sequence in Fig.**2a**, and its value was of $\nu_{off} = 300$ kHz. On the ^{27}Al channel, except for the QFS irradiation, all pulses selectively excited the CTs. The maximum overall transfer efficiency was significantly enhanced by PT-*J*-HMQC (Fig.**11c**). Moreover, the optimal mixing time of PT-*J*-HMQC was shortened by a factor of ca. 1.7 compared to *J*-HMQC. In Fig.**12**, we have represented the experimental 2D ^{31}P-{^{27}Al} 2D spectra of $AlPO_4$-14 acquired with QFS PT-*J*-HMQC (Fig.**12a**) and conventional *J*-HMQC (Fig.**12b**). Representative vertical slices from these 2D spectra are displayed in Fig.**13**. It must be noted that the application of this low rf-field of QFS ($\nu_{1max} \approx 14$ kHz) leads to the lower gain (1.8-2.1) of Al_1 compared with that (2.3-2.6) of the other three Al sites in PT-*J*-HMQC experiment. However, this gain is still higher than that (1.4 - 1.6) obtained by using DFS/DWURST schemes at the same conditions (results not shown). It must be noted that our previous study showed that the maximum efficiency was observed with PT-*J*-HMQC when ν_{off} was set at the most intense sideband of ST_1 [22b], and the efficiency dropped when ν_{off} was small.

Nevertheless, these results demonstrate that the quadruple sweep strategy always leads to an improved robustness of ST $\rightarrow$ CT transfer to accelerate the *J* recoupling between the two nuclei, which improves the sensitivity when used with the *J*-HMQC

sequence due to reduced losses.

Conclusion

In this work, we have demonstrated the advantages of the improved strategy of STs manipulation by using the quadruple frequency sweep technique. Instead of sweeping only one pair of symmetrical ST spinning sidebands, sweeping two different such pairs makes the ST $\rightarrow$ CT transfer much less sensitive to the offset of the sweep pulses. This method, which only requires 6% more rf-power than the double sweep, allows manipulating efficiently the STs of several sites with quite different C_Q values, thus achieving similar signal enhancements for samples containing several nonequivalent sites. This robustness with respect to C_Q is simultaneously obtained with a good robustness with respect to the sweeping rf-field. Both advantages are mandatory when analyzing samples whose spectra have a low S/N ratio. Indeed, it is then very difficult and time consuming to optimize carefully the rf-field and offset parameters.

We have demonstrated this strategy in the case of pulse-acquire 1D experiments, and shown that it can also be employed in our recently developed PT-*J*-HMQC 2D experiment. This scheme can also be combined with many other 2D experiments involving half-integer quadrupolar nuclei to improve the experimental sensitivity. We have proposed two quadruple frequency sweep techniques based on sideband-selective DFS and WURST excitations, called QFS and QWURST, respectively. We have shown that (i) both sweepings provide the same signal gain of ca. 2.5, independent on the C_Q value, but (ii) that QFS is slightly more robust than QWURST with respect to the offset, hence requiring less offset optimization.

ACKNOWLEDGMENTS:

The Chinese authors are grateful for the funding supported by "National Natural Science Foundation of China (21733013, 21573278, 91745111, 21611130104 and 21622311)". J. Trébosc, O. Lafon and J.-P. Amoureux are grateful for funding provided by Region Nord/Pas de Calais, Europe (FEDER), CNRS, French Minister of Science, USTL, ENSCL, CortecNet, and contract ANR-2010-jcjc-0811-01. Financial

support from the IR-RMN-THC Fr-3050 CNRS for conducting the research is gratefully acknowledged.

Reference:

[1] (a) S.E. Ashbrook, Recent advances in solid-state NMR spectroscopy of quadrupolar nuclei, *Phys. Chem. Chem. Phys.,* 11 (**2009**) 6892-6905; (b) S.E. Ashbrook, S. Sneddon, New Methods and Applications in Solid-State NMR Spectroscopy of Quadrupolar Nuclei, *J. Am. Chem. Soc*., 136 (**2014**) 15440-15456.

[2] C. Fernandez, M. Pruski, Probing quadrupolar nuclei by solid-state NMR spectroscopy: recent advances, *Top. Curr. Chem*., 306 (**2012**) 119-188.

[3] (a) A. Samoson, E. Kundla, E. Lippmaa, High-resolution MAS-NMR of quadrupolar nuclei in powders, *J. Magn. Reson*., 49 (**1982**) 350-357; (b) A. Samoson, E. Lippmaa, Excitation phenomena and line-intensities in high-resolution NMR powder spectra of half-integer quadrupolar nuclei, *Phys. Rev. B*, 28 (**1983**) 6567-6570.

[4] C.A. Fyfe, Y. Feng, H. Grondey, G.T. Kokotailo, H. Gies, One- and two-dimensional high-resolution solid-state NMR studies of zeolite lattice structures, *Chem. Rev*., 91 (**1991**) 1525-1543.

[5] X.Q. Kong, L.A. O'Dell, V. Terskikh, E. Ye, R.Y. Wang, G. Wu, Variable-temperature 17O NMR studies allow quantitative evaluation of molecular dynamics in organic solids, *J. Am. Chem. Soc*., 134 (**2012**) 14609-14617.

[6] (a) F.A. Perras, D.L. Bryce, Direct investigation of covalently bound chlorine in organic compounds by solid-state 35Cl NMR spectroscopy and exact spectral line-shape simulations, *Angew. Chem.-Int. Edit*., 51 (**2012**) 4227-4230; (b) F.A. Perras, J. Viger-Gravel, K.M.N. Burgess, D.L. Bryce; Signal enhancement in solid-state NMR of quadrupolar nuclei, *Solid State Nucl. Magn. Reson*., 51-52 (**2013**) 1-15.

[7] G. Wu, J.F. Zhu, NMR studies of alkali metal ions in organic and biological solids, *Prog. Nucl. Magn. Reson. Spectrosc.,* 61 (**2012**) 1-70.

[8] (a) P. Gao, Q. Wang, J. Xu, G.D. Qi, C. Wang, X Zhou, X.L. Zhao, N.D. Feng, X.L. Liu, F. Deng, Brønsted/Lewis acid synergy in methanol-to-aromatics conversion on Ga-modified ZSM-5 zeolites, as studied by solid-state NMR spectroscopy, *ACS Catal.* 8 **(2018)** 69-74; (b) H. Nagashima, J. Trébosc, L. Calvez, F. Pourpoint, F. Mear, O. Lafon, J.-P. Amoureux, 71Ga-77Se connectivities and proximities in gallium selenide crystal and glass probed by solid-state NMR, *J. Magn. Reson.*, 282 (**2017**) 71-82.

[9] T.T. Nakashima, R.E. Wasylichen, Sensitivity and resolution enhancement of half-integer quadrupolar nuclei in solid-state NMR, *eMagRes*, **2011**.

[10] (a) P.K. Madhu, A. Goldbourt, L. Frydman, S. Vega, Fast radio-frequency amplitude modulation in multiple-quantum magic-angle-spinning nuclear magnetic resonance: theory and experiments, *J. Chem. Phys.*, 112 (**2000**) 2377-2391; (b) R. Siegel, T.T. Nakashima, R.E. Wasylichen, Sensitivity enhancement of NMR spectra of half‐integer quadrupolar nuclei in the solid state via population transfer, *Concepts Magn. Reson*., 26A (**2005**) 47-61.

[11] (a) S. Vega, Y. Naor, Triple quantum NMR on spin systems with I = 3/2 in solids, *J. Chem. Phys*., 75 (**1981**) 75; (b) J. Haase, M.S. Conradi, Sensitivity enhancement for NMR of the central transition of quadrupolar nuclei, *Chem. Phys. Lett*., 209 (**1993**) 287-291; (c) R. Siegel, T.T. Nakashima, R.E. Wasylichen, Signal enhancement of NMR spectra of half-integer quadrupolar nuclei in solids using hyperbolic secant pulses, *Chem. Phys. Lett*., 388 (**2004**) 441-445.

[12] (a) T. Brauniger, K. Ramaswamy, P.K. Madhu, Enhancement of the central-transition signal in

static and magic-angle-spinning NMR of quadrupolar nuclei by frequency-swept fast amplitude-modulated pulses, *Chem. Phys. Lett*., 383 (**2004**) 403-410. (b) T. Brauniger, G. Hempel, P.K. Madhu, Fast amplitude-modulated pulse trains with frequency sweep (SW-FAM) in static NMR of half-integer spin quadrupolar nuclei, *J. Magn. Reson*., 181 (**2006**) 68-78; (c) T. Brauniger, Enhancing the central-transition NMR signal of quadrupolar nuclei by spin population transfer using SW-FAM pulse trains with a tangent-shaped sweep profile, *Solid State Nucl. Magn. Reson*., 45-46 (**2012**) 16-22.

[13] A.P.M. Kentgens, R. Verhagen, Advantages of double frequency sweeps in static, MAS and MQMAS NMR of spin I = 3/2 nuclei, *Chem. Phys. Lett*., 300 (**1999**) 435-443.

[14] E. Van Veenendal, B.H. Meier, A.P.M. Kentgens, Frequency stepped adiabatic passage excitation of half-integer quadrupolar spin systems, *Mol. Phys*., 93 (**1998**) 95.

[15] D. Iuga, A.P.M. Kentgens, Influencing the satellite transitions of half-integer quadrupolar nuclei for the enhancement of magic angle spinning spectra, *J. Magn. Reson*. 158 (**2002**) 65-72.

[16] (a) P. Caravatti, G. Bodenhausen, R.R. Ernst, Selective pulse experiments in high-resolution solid state NMR, *J. Magn. Reson*. 55 (**1983**) 88-103; (b) A.J. Pell, G. Kervern, L. Emsley, M. Deschamps, D. Massiot, P.J. Grandinetti, G. Pintacuda, Broadband inversion for MAS NMR with single-sideband-selective adiabatic pulses, *J. Chem. Phys*., 134 (**2011**) 024117; (c) M. Shen J. Trébosc, O. Lafon, Z.H. Gan, F. Pourpoint, B. Hu, Q. Chen, J.-P. Amoureux, Solid-state NMR indirect detection of nuclei experiencing large anisotropic interactions using spinning sideband-selective pulses, *Solid State Nucl. Magn. Reson*. 72 (**2015**) 104-117.

[17] Z. Yao, H.T. Kwak, D. Sakellariou, L. Emsley, P.J. Grandinetti, Sensitivity enhancement of the central transition NMR signal of quadrupolar nuclei under magic-angle spinning, *Chem. Phys. Lett*., 327 (**2000**) 85-90.

[18] R. Siegel, T.T. Nakashima, R.E. Wasylishen, Signal enhancement of NMR spectra of half-integer quadrupolar nuclei in solids using hyperbolic secant pulses, *Chem. Phys. Lett*., 388 (**2004**) 441-445.

[19] K.K. Dey, S. Prasad, J.T. Ash, M. Deschamps, P.J. Grandinetti, Spectral editing in solid-state MAS NMR of quadrupolar nuclei using selective satellite inversion, *J. Magn. Reson*., 185 (**2007**) 326-330.

[20] (a) T.T. Nakashima, R.E. Wasylishen, R. Siegel, K.J. Ooms, Sensitivity enhancement of solid-state NMR spectra of half-integer spin quadrupolar nuclei: double- or single-frequency sweeps? Insights from the hyperbolic secant experiment, *Chem. Phys. Lett*. 450 (**2008**) 417-421; (b) M. Goswami, P.J.M. van Bentum, A.P.M. Kentgens, Sensitivity enhancement in MAS NMR of half-integer quadrupolar nuclei using sideband selective double-frequency sweeps, *Can. J. Chem*. 89 (**2011**) 1130-1137.

[21] (a) H. Kwak, S. Prasad, T. Clark, P. J. Grandinetti, Enhancing sensitivity of quadrupolar nuclei in solid-state NMR with multiple rotor assisted population transfers, *Solid State Nucl. Magn. Reson*. 24 (**2003**) 71-77. (b) M. Goswami, P.K. Madhu, Sensitivity enhancement of the central-transition signal of half-integer spin quadrupolar nuclei in solid-state NMR: Features of multiple fast amplitude-modulated pulse transfer, *J. Magn. Reson*., 192 (**2008**) 230-234. (c) M. Goswami, P.J.M. van Bentum, A.P.M. Kentgens, Repetitive sideband-selective double frequency sweeps for sensitivity enhancement of MAS NMR of half-integer quadrupolar nuclei, *J. Magn. Reson*., 219 (**2012**) 25-32.

[22] (a) Q. Wang, J. Trébosc, Y. Li, J. Xu, B. Hu, N. Feng, Q. Chen, O. Lafon, J.-P. Amoureux, F. Deng, Signal enhancement of *J*-HMQC experiments in solid-state NMR involving half-integer quadrupolar nuclei, *Chem. Commun.*, 49 (**2013**) 6653-6655; (b) Q. Wang, Y. Li, J. Trébosc, O. Lafon, J. Xu, B. Hu, N. Feng, Q. Chen, J.-P. Amoureux, F. Deng, Population transfer HMQC for half-integer quadrupolar nuclei, *J. Chem. Phys*., 142 (**2015**).

[23] (a) H.-T. Kwak, S. Prasad, T. Clark, P.J. Grandinetti, Selective suppression and excitation of

solid-state NMR resonances based on quadrupole coupling constants, *J. Magn. Reson*. 160 (**2003**) 107-113; (b) T.T. Nakashima, R. Teymoori, R.E. Wasylishen, Using hyperbolic secant pulses to assist characterization of chemical shift tensors for half-integer spin quadrupolar nuclei in MAS powder samples, *Magn. Reson. Chem*. 47 (**2009**) 465-471.

[24] (a) E. Kupče, R. Freeman, Adiabatic pulses for wideband inversion and broadband decoupling, *J. Magn. Reson*., A115 (**1995**) 273-276; (b) L. O'Dell, The WURST kind of pulses in solid-state NMR, *Solid State Nucl. Magn. Reson*., 55 (**2013**) 28-41.

[25] M. Garwood, L. DelaBarre, The return of the frequency sweep: designing adiabatic pulses for contemporary NMR, *J. Magn. Reson*., 153 (**2001**) 155-177.

[26] J. Trébosc, J.-P. Amoureux, Z. Gan, Comparison of high-resolution solid-state NMR MQMAS and STMAS methods for half-integer quadrupolar nuclei, *Solid State Nucl. Magn. Reson*., 31 (**2007**) 1-9.

[27] M. Bak, J.T. Rasmussen, N.C. Nielsen, SIMPSON: a general simulation program for solid-state NMR spectroscopy, *J. Magn. Reson*., 147 (**2000**) 296-330.

[28] M. Bak, N.C. Nielsen, REPULSION, a novel approach to efficient powder averaging in Solid-State NMR, *J. Magn. Reson*., 125 (**1997**) 132-139.

[29] S. Antonijevic, S.E. Ashbrook, S. Biedasek, R.I. Walton, S. Wimperis, H.X. Yang, Dynamics on the microsecond timescale in microporous aluminophosphate $AlPO_4$-14 as evidenced by ^{27}Al MQMAS and STMAS NMR spectroscopy, *J. Am. Chem. Soc*., 128 (**2006**) 8054-8062.

[30] D. Massiot, F. Fayon, B. Alonso, J. Trébosc, J.-P. Amoureux, Chemical bonding differences evidenced from J-coupling in solid state NMR experiments involving quadrupolar nuclei, *J. Magn. Reson*., 164 (**2003**) 160-164.

[31] L. Delevoye, J. Trébosc, Z. Gan, L. Montagne, J.-P. Amoureux, Resolution enhancement using a new multiple-pulse decoupling sequence for quadrupolar nuclei, *J. Magn. Reson*., 186 (**2007**) 94-99.

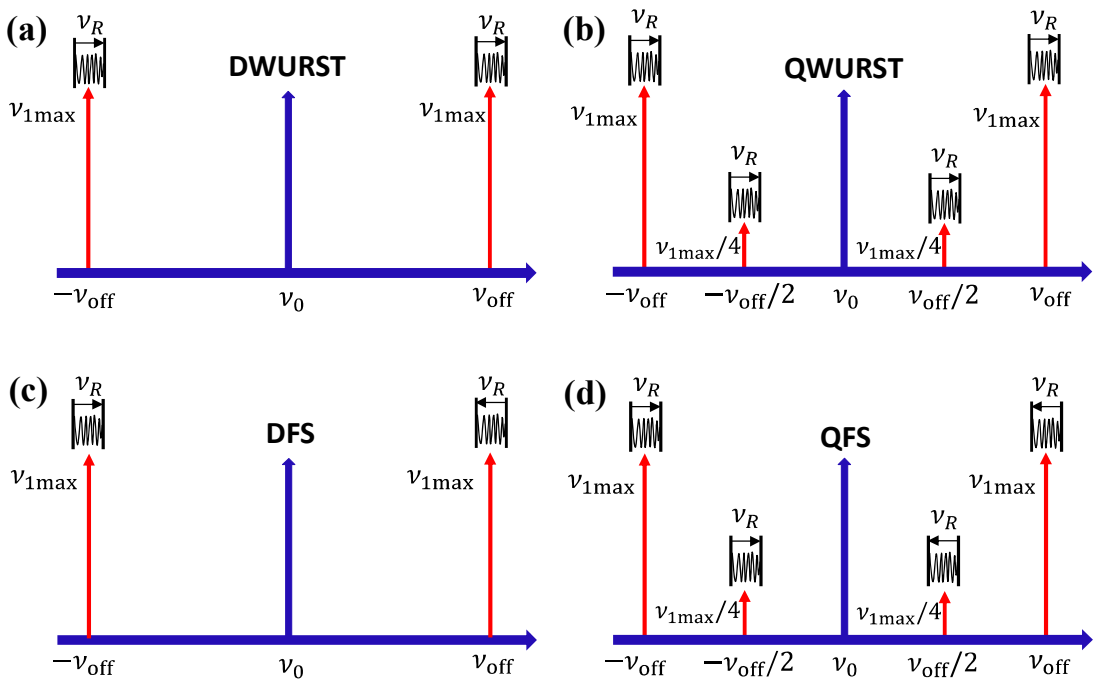

Fig.1. Schematic representations of adiabatic frequency sweeps. Double frequency sweeps: DWURST (a) and DFS (c); Quadruple frequency sweeps: QWURST (b) and QFS (d).

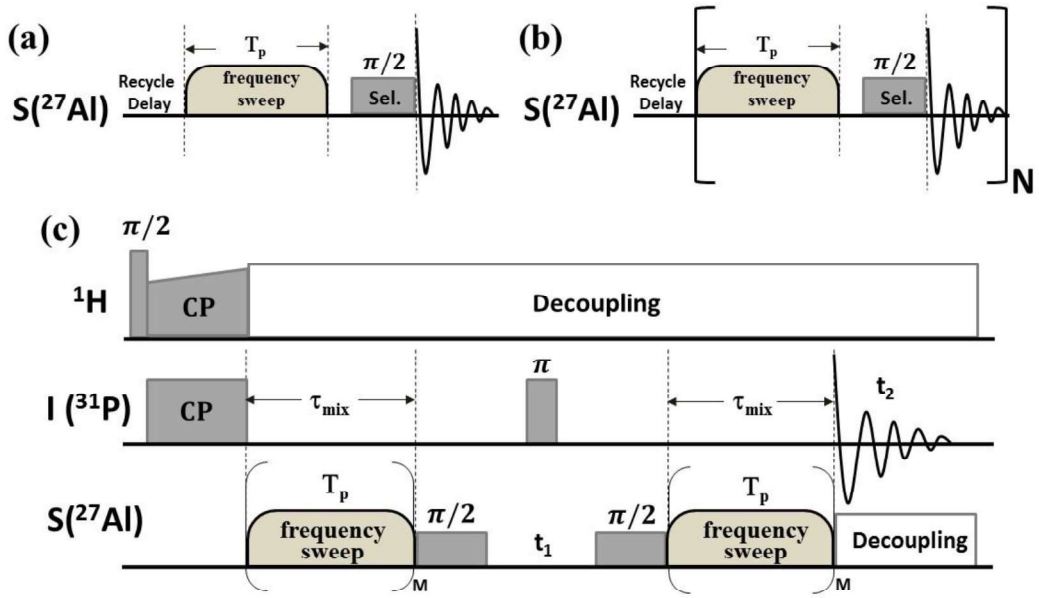

Fig.2. (a) Pulse sequence for CT signal enhancement of half-integer quadrupolar nuclei with initial ST saturation/inversion. (b) Repetitive QFS-CT selective sequence with N acquisitions. (c) Pulse scheme for I-{S > 1/2} PT-*J*-HMQC experiment with the initial magnetization of I spins generated by cross-polarization (CP) from protons. During the J_{IS} defocusing and refocusing delays, τ_{mix}, the polarization transfer is accelerated by applying M frequency-swept pulses of T_p length each to manipulate STs of S spins.

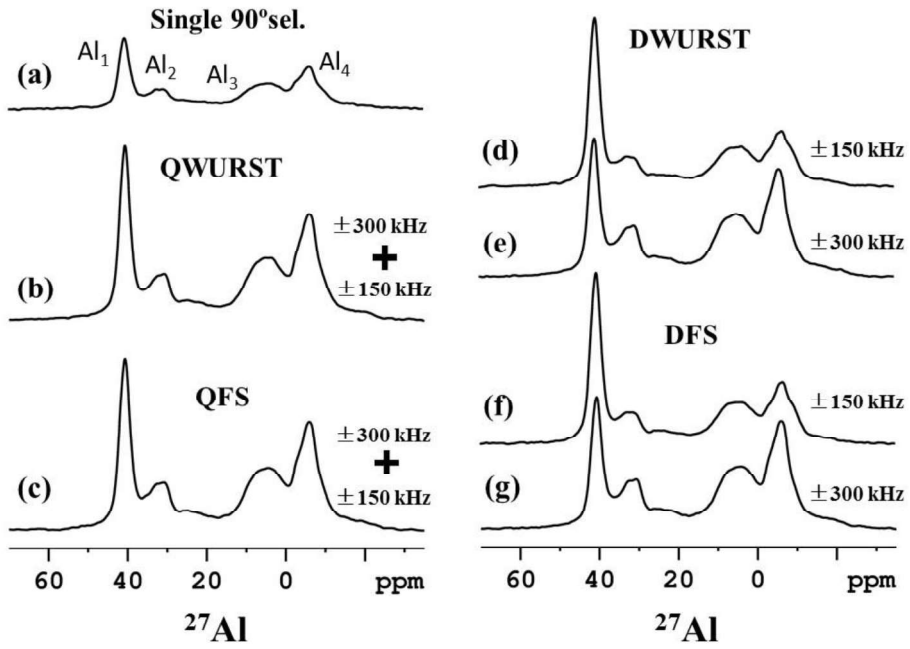

Fig.3. $AlPO_4$-14 ^{27}Al 1D MAS spectra obtained with π/2-CT-selective pulse: (a) alone, or (b-g) preceded with STs manipulation by QWURST (b), QFS (c), DWURST (d,e), DFS (f,g) with ν_{1max} = 26.4 kHz, ν_{off} = 150 (d,f), 300 (e,g) or 150 and 300 (b,c) kHz (indicated on the spectra). B_0 = 9.4 T, ν_R = 15 kHz, T_p = 500 μs, 16 scans with a relaxation delay of 2 s.

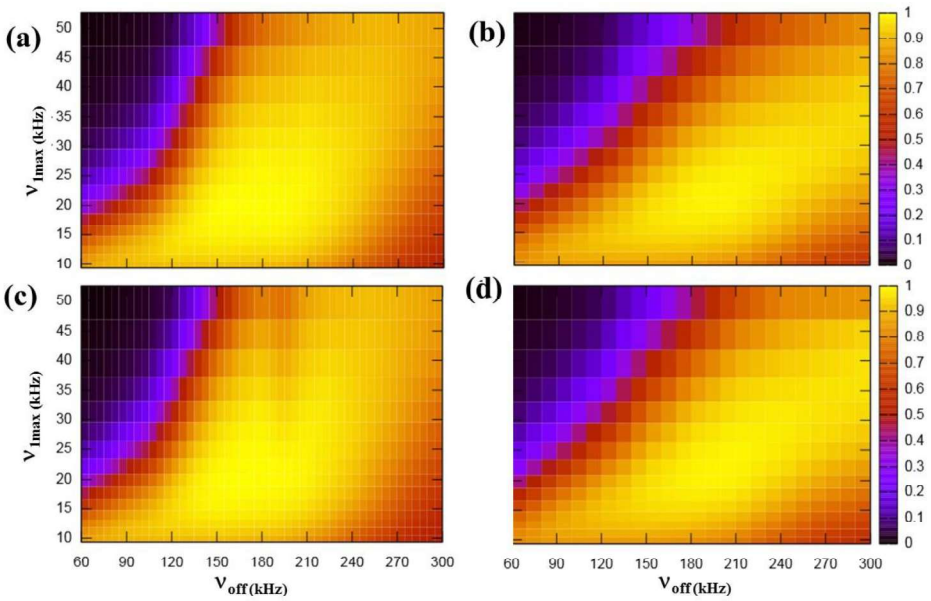

Fig.4. $AlPO_4$-14 Al_1 (C_Q = 1.7 MHz) normalized signal versus ν_{1max} and ν_{off} in MAS spectra obtained with sequences shown in Fig.**2a** with sweeps either at $\pm\nu_{off}$ with (a) DWURST and (c) DFS, or $\pm\nu_{off}$ and $\pm\nu_{off}/2$ with (b) QWURST and (d) QFS. B_0 = 9.4 T, ν_R = 15 kHz and T_p = 500 μs.

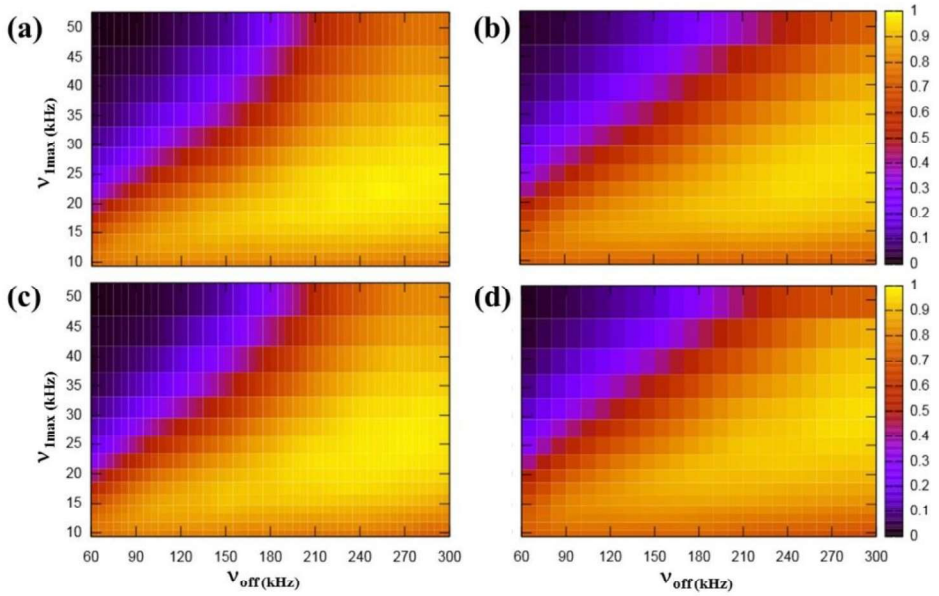

Fig.5. $AlPO_4$-14 Al_3 (C_Q = 5.6 MHz) normalized signal versus ν_{1max} and ν_{off} in MAS spectra obtained with sequences shown in Fig.**2a** with sweeps either at $\pm\nu_{off}$ with (a) DWURST and (c) DFS, or $\pm\nu_{off}$ and $\pm\nu_{off}/2$ with (b) QWURST and (d) QFS. B_0 = 9.4 T, ν_R = 15 kHz and T_p = 500 μs.

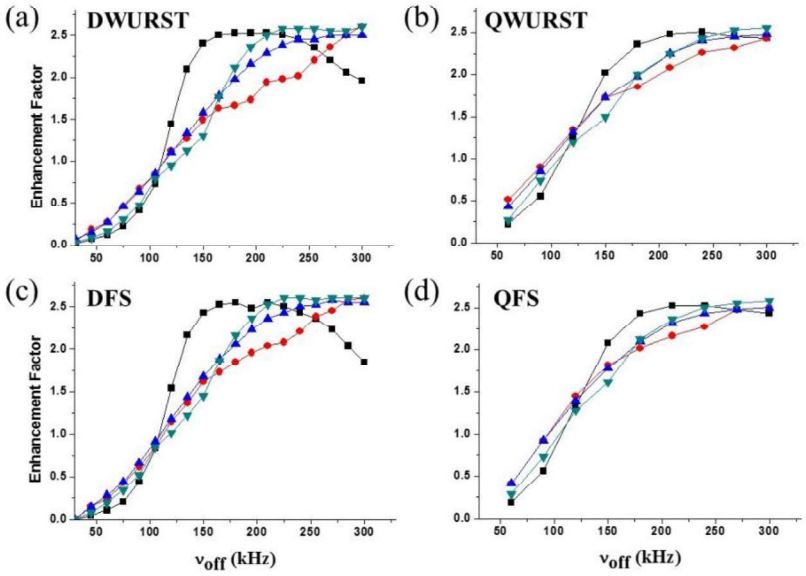

Fig.6. $AlPO_4$-14 experimental enhancement factor for the four ^{27}Al sites (Al_1: -■-, Al_2: -●-, Al_3: -▲-, Al_4: -▼-) versus ν_{off} with: (a) DWURST, (b) QWURST, (c) DFS and (d) QFS. $B_0 = 9.4$ T, $\nu_R = 15$ kHz, $T_p = 500$ µs and $\nu_{1max} = 26.4$ kHz.

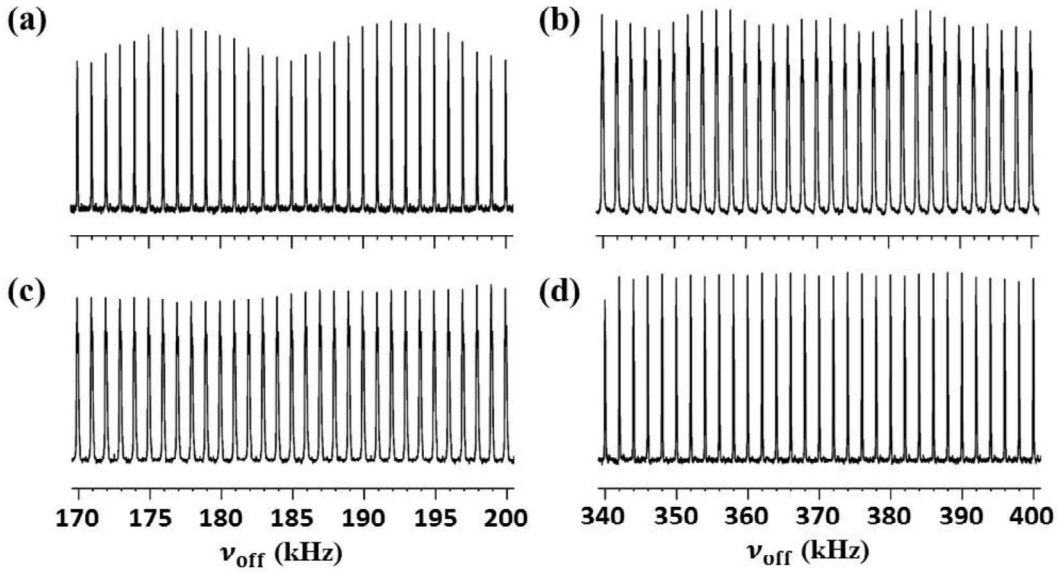

Fig.7. Berlinite experimental ^{27}Al CT-signal optimization versus ν_{off} of sequence in Fig.**2a** with: (a) DWURST, (b) QWURST, (c) DFS, (d) QFS. B_0 = 9.4 T, ν_R = 15 kHz, T_p = 500 μs, ν_{1max} = 26.4 kHz and NS = 16.

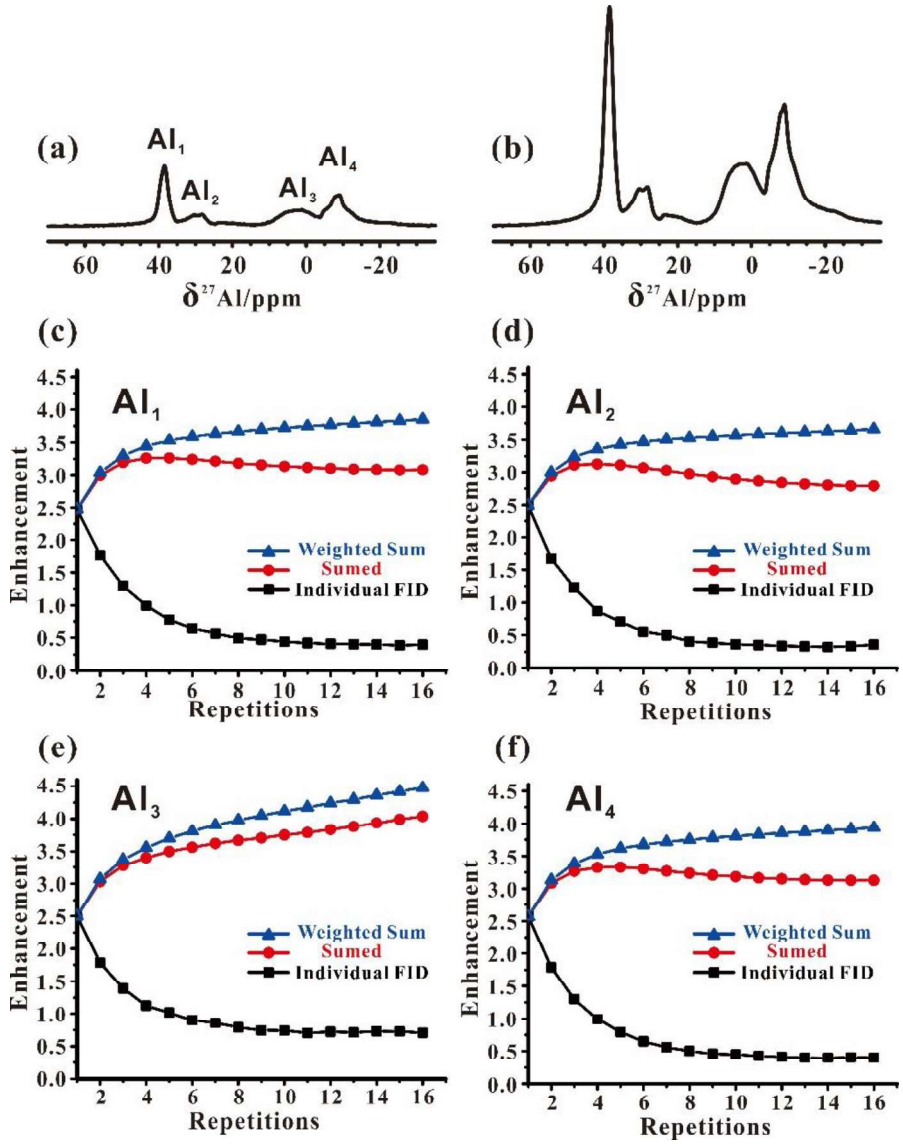

Fig.8. Experimental ^{27}Al MAS spectra of $AlPO_4$-14 obtained using: (a) a $\pi/2$-CT-selective pulse, (b) a repetitive QFS adding N = 16 individual FIDs acquired with the sequence shown in Fig.2b. Statistic enhancement of the four ^{27}Al sites (c-f) with repetitive QFS: black squares: S/N for each of the N individual FIDs; red circles: enhancement of S/N if the sum of the N individual FIDs is used; blue triangles: enhancement of S/N for the weighted sum of the N individual FIDs. B_0 = 9.4 T, ν_R = 15 kHz, T_p = 500 µs, ν_{1max} = 26.4 kHz and a relaxation delay of 2 s.

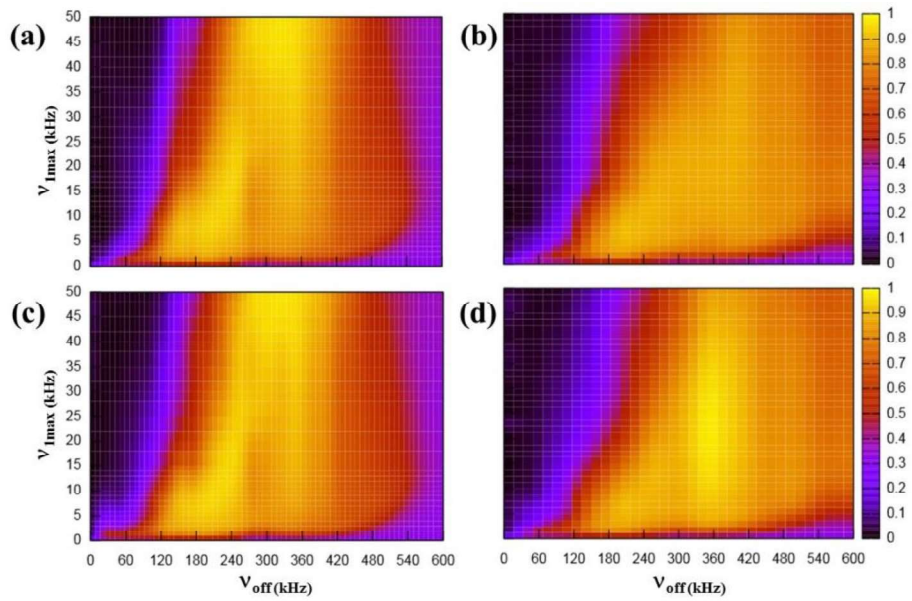

Fig.9. Simulation results of the normalized signal intensities of $^{31}P \rightarrow {}^{27}Al \rightarrow {}^{31}P$ transfer in PT-*J*-HMQC experiments for one isolated ^{27}Al-^{31}P spin-pair with J = 100 Hz and $\mathbf{C_Q = 3.0}$ MHz as a function of peak rf-field (ν_{1max}) and offset (ν_{off}) obtained by the pulse sequence described in Fig.**2c** with different frequency sweeps: (a) DWURST, (b) QWURST, (c) DFS and (d) QFS. B_0 = 9.4 T, τ_{mix} = 1.68 ms ≈ 1/6J, ν_R = 25 kHz and T_p = 500 μs.

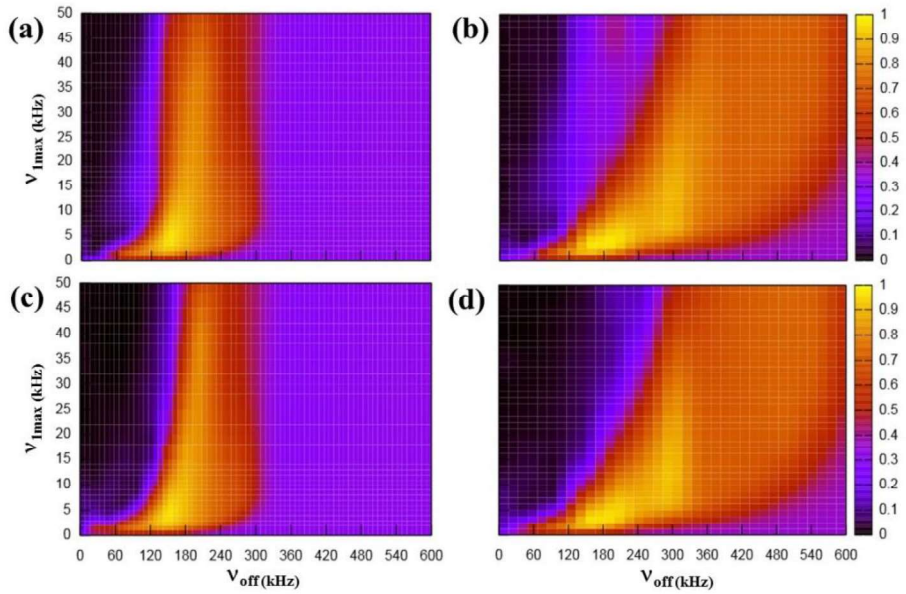

Fig.10. Simulation results of the normalized signal intensities of $^{31}P \rightarrow {}^{27}Al \rightarrow {}^{31}P$ transfer in PT-*J*-HMQC experiments for one isolated ^{27}Al-^{31}P spin-pair with J = 100 Hz and $\mathbf{C_Q = 1.5}$ MHz as a function of peak rf-field (ν_{1max}) and offset (ν_{off}) obtained by the pulse sequence described in Fig.**2c** with different frequency sweeps: (a) DWURST, (b) QWURST, (c) DFS and (d) QFS. B_0 = 9.4 T, τ_{mix} = 1.68 ms ≈ 1/6J, ν_R = 25 kHz and T_p = 500 μs.

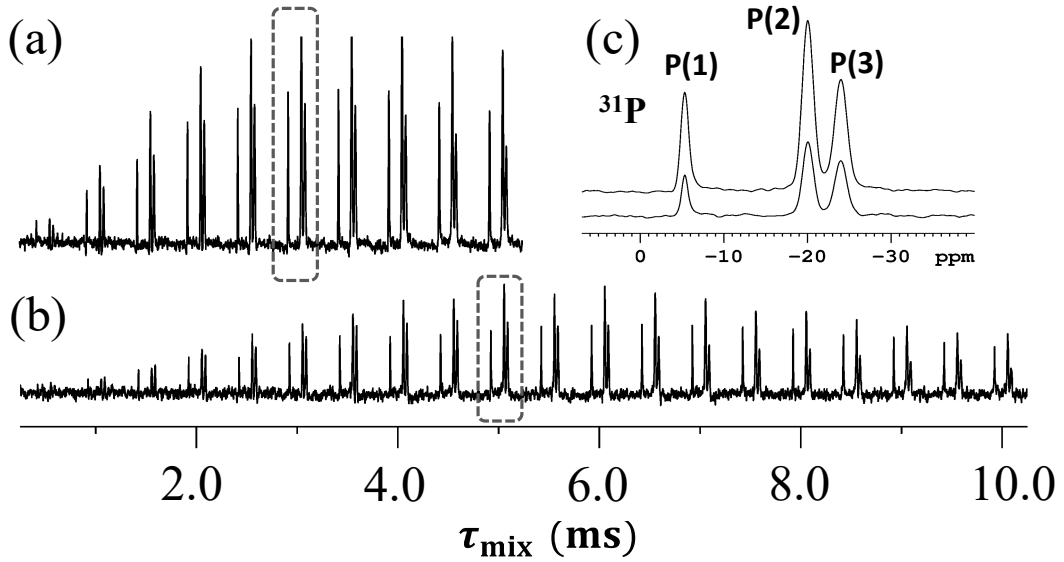

Fig.11. $AlPO_4$-14 ^{31}P-{^{27}Al} 1D ($t_1 = 0$) spectra at $B_0 = 9.4$ T with $\nu_R = 15$ kHz. ^{31}P signal intensities versus τ_{mix} for (a) PT-*J*-HMQC (Fig.**2c**) with QFS using $T_p = 500$ μs, $\nu_{off} = 300$ kHz and $\nu_{1max} = 14$ kHz, and (b) conventional *J*-HMQC. (c) Expansion of optimal ^{31}P spectra obtained with (b) ($\tau_{mix} = 5.0$ ms) and (a) ($\tau_{mix} = 3.0$ ms) experiments, respectively.

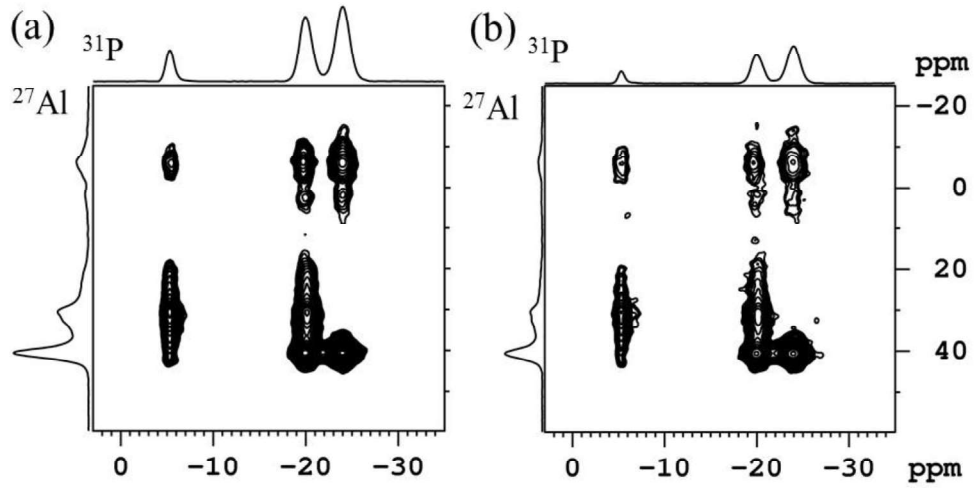

Fig.12. $AlPO_4$-14 ^{31}P-{^{27}Al} *J*-HMQC TPPI spectra at B_0 = 9.4 T with ν_R = 15 kHz, T_p = 500 μs, TD (F1) = 140, Δt_1 = 66.67 μs, NS = 16, D1 = 2 s, experimental time ≈ 1.3 h, and skyline projections along F1 and F2. These spectra have been obtained: (a) with QFS (ν_{1max} = 14 kHz) and τ_{mix} = 3.0 ms, and (b) conventional sequence with τ_{mix} = 5.0 ms, and they are represented with same contour levels.

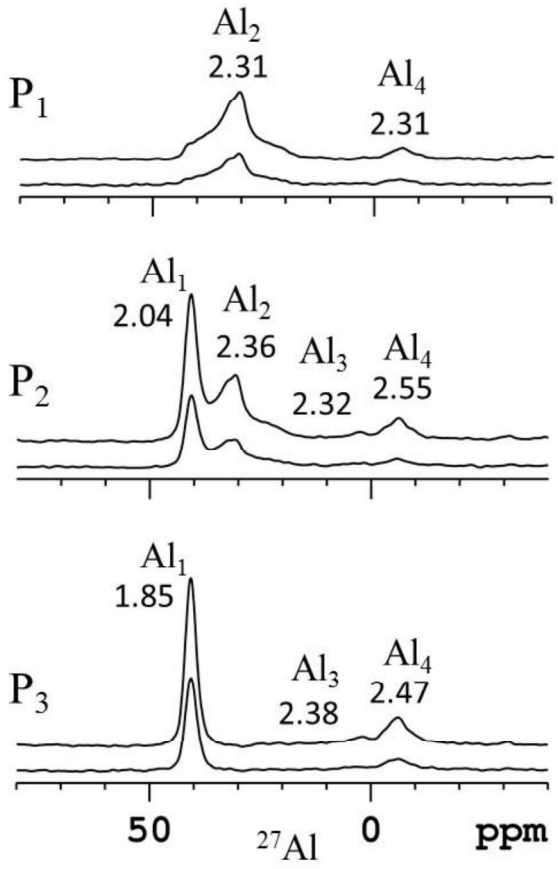

Fig.13. Experimental representative slices along F1 of Fig.**12** for the three ^{31}P sites obtained by conventional *J*-HMQC (bottom) and PT-*J*-HMQC with QFS (top) experiments. The numbers are the sensitivity gains of the different ^{27}Al sites obtained by QFS sweeps with respect to the conventional *J*-HMQC experiment.

Table 1. Enhancement factors of the four Al sites on $AlPO_4$-14 with different sweep schemes by using the pulse sequence in Fig.2a.

ν_{1max} = 26.4 kHz	C_Q (MHz)	QWURST	QFS	DWURST		DFS	
ν_{off} (kHz)		300 + 150	300 + 150	300	150	300	150
Al_1	1.7	2.45	2.43	1.85	2.40	1.84	2.43
Al_2	4.2	2.43	2.50	2.65	1.49	2.60	1.61
Al_3	5.6	2.47	2.50	2.50	1.58	2.54	1.64
Al_4	2.6	2.55	2.57	2.58	1.35	2.59	1.44